Atomistic simulations of amorphous alumina surfaces

S. P. Adiga,[1] P. Zapol,[1,2,*] and L. A. Curtiss[1,2]
[1]*Materials Science Division, 9700 South Cass Avenue, Argonne National Laboratory, Argonne, Illinois 60439, USA*
[2]*Chemistry Division, 9700 South Cass Avenue, Argonne National Laboratory, Argonne, Illinois 60439, USA*
(Received 24 February 2006; revised manuscript received 10 May 2006; published 17 August 2006)

The surface structure of amorphous Al_2O_3 has been studied using atomistic molecular dynamics simulations. The density profiles indicate that oxygen is preferred at the surface causing Al enrichment just below (<2 Å) the surface. Distributions of coordination numbers, bondlengths and bond angles indicate that edge sharing Al tetrahedra configurations are more preferred at the surface than in the bulk. Structural differences of amorphous and crystalline alumina surfaces are discussed.

DOI: 10.1103/PhysRevB.74.064204 PACS number(s): 61.43.−j, 68.35.−p, 68.47.Gh

I. INTRODUCTION

Understanding the structure of amorphous alumina is of considerable interest because of its role in many technologically important applications such as catalysts, catalytic supports, and dielectric barriers. Amorphous alumina can be produced in a number of ways. For example, anodic oxidation of aluminum in an acidic environment is a well known technique that produces porous amorphous alumina membranes with pore diameters as small as 30 nm.[1] Recently, atomic layer deposition (ALD) was used to modify nanoporous anodic aluminum oxide membranes with a very precise pore size control, shrinking down their diameters to below ten nanometers with a narrow distribution.[2,3] The ability to design AAO membranes with tailor-made compositions and pore sizes has generated a great interest for use in heterogeneous catalysis.[3] Additionally, ALD of Al_2O_3 has been used to form amorphous thin films for potential applications as a high-k dielectric material.[4]

In the applications mentioned above, the surfaces and interfaces of amorphous alumina layers have a major effect on their functionality. Therefore, it is important to gain an understanding of the surface structure in terms of the local atomic arrangement. First, information on the structure with respect to coordination number and short range order is essential in identifying binding sites on the surface of amorphous alumina catalytic supports. Second, this understanding is central in developing a detailed description of film growth by ALD as both the rate and mechanism of growth are thought to be dependent on the surface structure.

The majority of the existing computational studies of alumina surfaces have considered various crystalline polymorphs including corundum (α-alumina) and transition aluminas (e.g., γ- and κ-alumina). Because the surface structures of these crystalline forms of alumina are well established, computational investigations of catalytic reactions[5] and ALD growth[6] on alumina surfaces have approximated the amorphous alumina surface with one of the forms of crystalline alumina surface. However, it is not evident that the structure and properties of these highly ordered surfaces represent those of amorphous alumina since coordination numbers, site distribution, and surface energies can be quite different in these two cases. Therefore, computational studies of amorphous alumina surfaces are vital to the understanding of their surface chemistry and provide realistic models of these materials. In the past, atomistic molecular dynamics (MD) simulations have proved to be successful in investigating surfaces of various amorphous materials. For example, MD simulations have provided complementary information to experimental surface analysis techniques in understanding the structure of amorphous silica surfaces.[7,8] While α- (Refs. 9 and 10) and γ- (Refs. 9 and 11) alumina surfaces and bulk amorphous alumina[12–15] have been studied using MD simulations, a comparable study of amorphous alumina surfaces does not exist.

In this work, molecular dynamics simulations have been performed using classical interatomic potentials to study amorphous alumina surfaces. The main goal of this paper is to investigate in detail the structural properties of amorphous alumina surfaces and to analyze how various structural features compare with corresponding properties of the bulk and crystalline alumina surfaces. In particular, the effect of the surface on density and concentration profiles is discussed. Further insight into the surface structure is gained by comparing the bondlength distribution, coordination numbers, partial radial distribution functions (PRDFs) and angle distributions for the surface and interior of the amorphous film.

II. SIMULATION DETAILS

MD simulations of amorphous alumina were performed as follows. The potential used to model the interatomic interactions of alumina is a pair potential of the Buckingham form along with partial charges on atoms, due to Matsui *et al.*[16] The details of the potential can be found elsewhere.[17] This potential has been previously used to study liquid[17] and amorphous[12] aluminas in the bulk by Gutierrez *et al.* All the simulations were carried out in a microcanonical ensemble. An MD time step of 3 fs and a short-range interaction cutoff of 12 Å were used. The long range Coulomb interactions were calculated using the Ewald summation method. The simulations were performed using the MOLDY MD code.[18]

To carry out a reliable investigation of an amorphous alumina surface structure, the suitability of the interatomic potential for surface studies needs to be evaluated. The (0001) surface of α-alumina was chosen to test the potentials since it has been widely studied using first principles as well as atomistic simulation methods. For example, Gomes *et al.*[19]

TABLE I. Relaxation of outermost layers of the α-alumina surface (%). d_{ii+1} is the spacing between ith and $i+1$th layer from the surface.

Atomic layer	Present work 36 layers	Ref. 19 B3LYP, 15 layers	Ref. 19 LDA
d_{12}	−61.4	−81.9	−89.2
d_{23}	4.5	−4.2	−0.2
d_{34}	−57.9	−37.1	−36.5
d_{45}	23.3	17.9	17.0

have reported structural relaxation of the α-alumina (0001) surface calculated from first principles using Hartree Fock and density functional theory (DFT) with both the local density approximation (LDA) and the hybrid B3LYP exchange-correlation functionals. MD simulations of the α-alumina (0001) surface were performed using the above mentioned interatomic potential and the surface relaxation was compared with previous first principles results in terms of changes in interlayer spacings. The bulk sample consisted of 2160 atoms in an orthorhombic simulation cell with the $\langle 0001 \rangle$ direction parallel to the z axis. The bulk α-alumina simulation box lengths were optimized to $a=28.3004$ Å, $b=24.5089$ Å, and $c=25.7493$ Å. The surfaces were created by abruptly increasing the periodic box in the z direction by 50 Å creating an Al-terminated slab of 36 layers. This slab was relaxed at 0 K. The surface relaxation obtained in this work is compared with previous first principles calculations in Table I. The MD results match quite well with first principles results considering that the latter vary depending on the model and the method used. The surface energy is the difference in total energy between the slab and the corresponding bulk sample divided by the total surface area of the slab. For α-alumina in this study, the surface energy was calculated to be 2.04 J/m^2 at 0 K. The majority of the theoretical calculations have reported surface energy values between 2.0 and 3.0 J/m^2.[20,21] The surface energy has been experimentally determined to be 2.6 J/m^2.[21] The results indicate that the interatomic potential produces a fairly accurate description of the structure and energy of this alumina surface, and it is a reasonable choice for alumina surface studies.

The bulk amorphous alumina sample was obtained using the following procedure. Initially, a total number of 2375 Al and O atoms in a ratio corresponding to stoichiometric Al_2O_3 are placed in an orthorhombic supercell of the hexagonal α-alumina lattice. Then, the volume of the MD periodic box was anisotropically scaled to $V=40\times40\times40$ Å^3. The system was heated to a temperature of 5000 K and equilibrated for 2×10^5 time steps. The sample was then quenched to 3000 K and equilibrated at this temperature for 10^5 time steps. It is useful to point out that this is still above both the melting point of about 2326 K and the glass transition temperature of about 2000 K[14] for amorphous alumina. Subsequently, the lengths of the periodic MD cell and the atomic positions were scaled simultaneously to create an Al_2O_3 sample of density 3.236 g/cm^3 that corresponded to simulation box lengths of $a=b=c=29.18$ Å. This density corresponds to a typical value observed experimentally.[12,22] Following this, the MD box was replicated three times in x and y directions such that the new system consisted of 21375 atoms and had box lengths of $a=b=87.54$ Å and $c=29.18$ Å. This was followed by quenching the system to 300 K through intermediate temperatures. Free surfaces were created by abruptly making the periodic box longer in the z direction by 50 Å after the amorphous bulk sample was obtained. This resulted in a periodically repeated slab of alumina of thickness 29.18 Å with two surfaces of area 87.54×87.54 Å^2 perpendicular to the z axis. Following the surface formation the thin film was relaxed at 1000 K for 1.2 ns to anneal the surface. Finally, simulations were carried out at 300 K for 1.2 ns. The system reached equilibration within the first 300 ps and the potential energy oscillated around an average value. The sampling was performed over the final 600 ps. A snapshot of the system that includes atoms from the top 3 Å layer is given in Fig. 1.

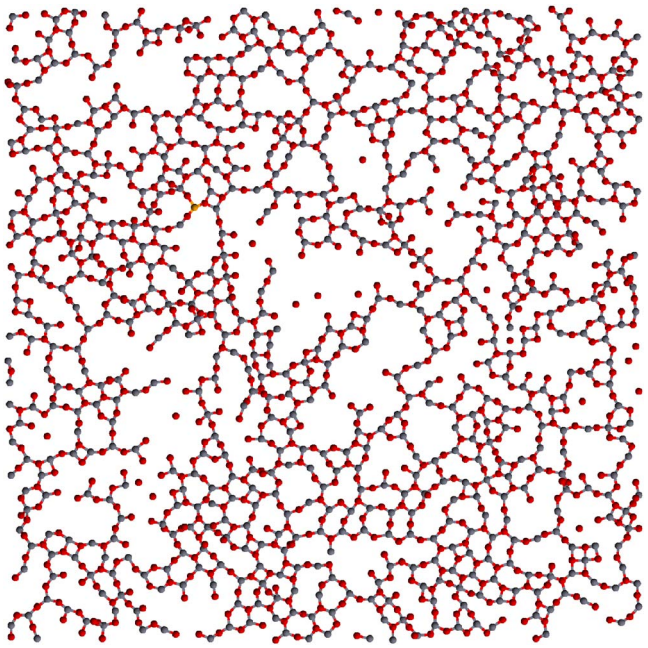

FIG. 1. (Color online) Snapshot of the top 3 Å layer of the model amorphous alumina surface.

III. RESULTS

A. Comparison of Al-O bondlength distribution in the bulk and surface

The properties of the bulk system are characterized in terms of PRDF, bondlength, and coordination number distributions to form a basis for surface simulations. Structural features of our bulk system can be directly compared with previous MD simulations on amorphous alumina by Gutierrez *et al.*[12] Their simulations have shown that amorphous alumina mainly consists of AlO_4 tetrahedra, connected to each other through a corner or edge sharing configuration. In their study, amorphous alumina at three different values of density was considered. The overall features of bulk amorphous alumina structure in this work are similar to those

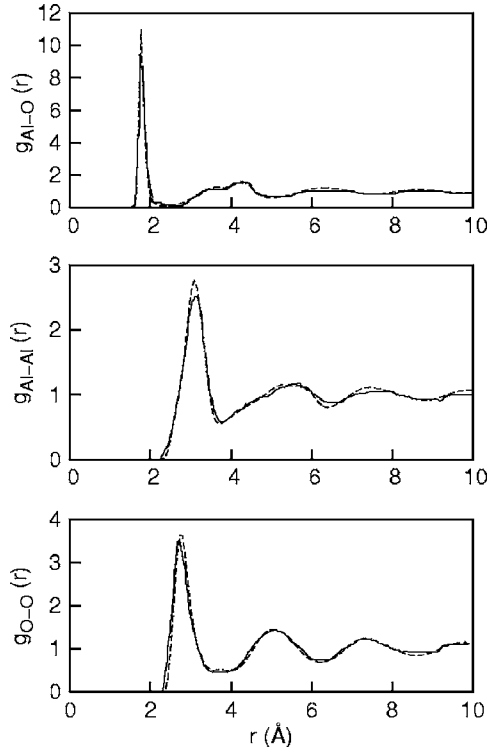

FIG. 2. Comparison of PRDF for bulk amorphous alumina from the present work (dotted) and Ref. 12 (solid).

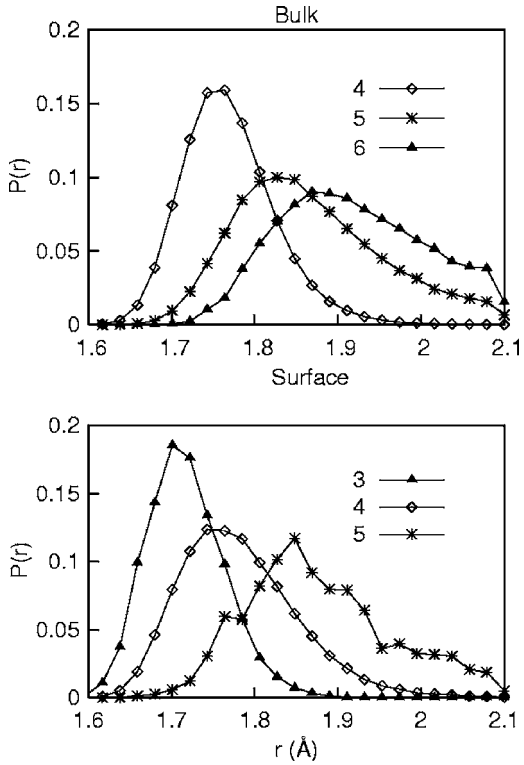

FIG. 3. Probability distribution of Al-O bondlength for four-, five-, and six-coordinated Al in the bulk amorphous alumina and for three-, four-, and five-coordinated Al in the top 3 Å layer of the amorphous alumina surface at $T=300$ K.

obtained for their system with density 3.175 g/cm^3 based on comparison of bulk PRDFs and coordination number distribution. The partial radial distribution function $g(r)$ is defined as

$$g_{\alpha\beta}(r) = \frac{\langle n_{\alpha\beta}(r,\Delta r)\rangle}{4\pi r^2 \Delta r \rho_\beta},$$

where $\langle n_{\alpha\beta}(r,\Delta r)\rangle$ is the average number of atoms of species β in a spherical shell of thickness Δr at a distance r from an atom of species α and ρ_β is the number density of atoms of species β. A value of $\Delta r=0.02$ Å is used. The $g_{\text{Al-O}}$, $g_{\text{Al-Al}}$, and $g_{\text{O-O}}$, for bulk amorphous alumina from this work are compared with the previous work in Fig. 2. The PRDF plots indicate a good match between the two studies. Further comparison can be carried out by determining the coordination number distribution. A cutoff distance of 2.1 Å for the Al-O bond distance derived from the position of the first minimum in the bulk $g_{\text{Al-O}}$ was used in the coordination number calculations. The fractions of four, five, and six coordinated Al in our sample are 0.74, 0.24, and 0.02, respectively. This compares well with the fractions 0.76, 0.22, and 0.02, respectively, of 4, 5, and 6 coordinated Al in amorphous Al_2O_3 of density of 3.175 g/cm^3 obtained by Gutierrez *et al.*[12] It is to be pointed out that the minor difference in coordination number distribution can be explained by the slightly higher density of our system.

The most important parameter that describes short range order in amorphous Al_2O_3 is the Al-O bondlength. Lamparter and Kneip[22] have reported x-ray and neutron scattering spectra on amorphous alumina films prepared by anodic oxidation. Using reverse Monte Carlo analysis they have calculated the RDF, and they have derived an average Al-O bondlength of 1.80 Å. This Al-O bondlength is smaller than the octahedral Al-O distances (1.86–1.97 Å) observed in α-Al_2O_3 and is larger than the tetrahedral Al(4)-O bondlength (1.73–1.78 Å) observed in transitional aluminas. The fraction of three, four, and five coordinated Al in their sample was 0.20, 0.56, and 0.22, respectively. The average Al-O distance provides a good indication of the average Al coordination number. The average Al-O bond distance in our bulk system was found to be 1.80 Å. To gain further insight on the dependence of Al-O bond distance on the coordination number of Al, the distribution of Al-O bondlength for four, five, and six coordinated Al for the bulk sample at 300 K (Fig. 3, top panel) is analyzed. Each bondlength distribution plot is normalized by the relative occurrence of Al of the respective coordination number. The Al(4)-O, Al(5)-O, and Al(6)-O bondlengths have peaks at 1.76, 1.83, and 1.88 Å, respectively. The bondlength distributions are narrower the lower the Al coordination number. A similar analysis can be carried out for the surface model considering atoms near the surface. The average Al-O bondlength for atoms in the top 3 Å layer is 1.78 Å. The decrease in average Al-O bondlength at the surface is due to three-coordinated Al atoms, which are absent in the bulk. In the bottom panel of Fig. 3, bondlength distributions for top 3 Å layer for the surface system is presented. The bondlength distributions for the surface layer are also characterized by the absence of Al(6)-O bonds as no six coordinated Al atoms are observed

in the surface layer. The distribution for three-coordinated Al has a peak at 1.70 Å. The Al(3)-O bondlength distribution is narrower compared to that for 4-coordinated Al. It can also be noted that the peak positions and shapes of distributions for Al(4)-O and Al(5)-O bondlengths remain unchanged for the surface.

It is useful to compare our calculations to the reverse Monte Carlo (RMC) results of Lamparter and Kniep.[22] In particular, they have reported fractions of 0.20, 0.56, and 0.22 for three-, four-, and five-coordinated aluminum atoms, respectively, and have concluded that the fraction of six-coordinated Al is very small, if present at all. A comparison to the respective values for our alumina bulk indicates agreement on the fraction of five-coordinated Al atoms. The rest of the Al atoms are mostly four-coordinated in our study but three- and four-coordinated in the RMC study. This discrepancy can possibly be explained by the high surface area of their sample, which is a porous alumina with 8% pore volume. As will be shown in a forthcoming section, the simulated surface structure has a considerable amount of three-coordinated Al. The bondlength distribution functions can be used to determine the average Al-O bondlength if the relative amount of three-, four-, five-, and six-coordinated Al are known. For example, for the fractions of three-, four-, and five-coordinated Al reported in Ref. 22 the average Al-O distance is calculated to be 1.79 Å using the bondlength distributions presented in Fig. 3. Here, we assume that the remaining 2% of the Al atoms are six-coordinated. This is in good agreement with the average value of 1.8 Å reported in Ref. 22.

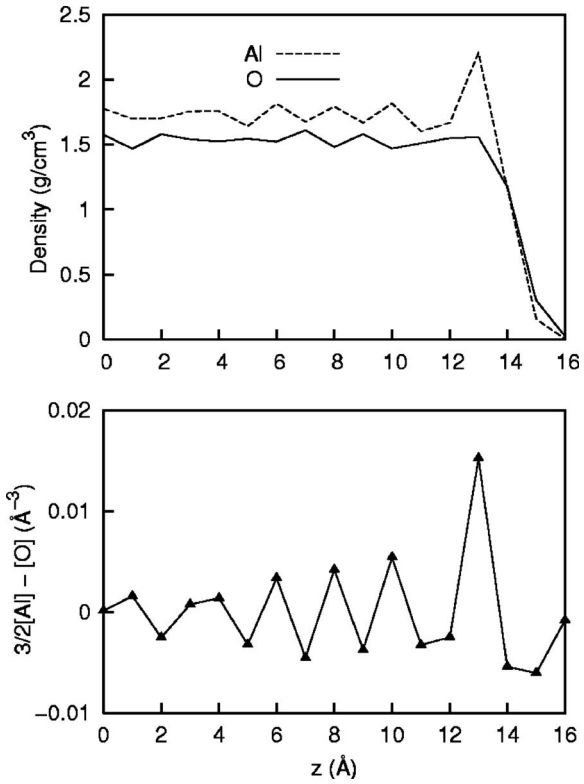

FIG. 4. Profiles of mass density (top) and the quantity $\Delta n = 3/2[\mathrm{Al}]-[\mathrm{O}]$ in the z direction as a function of distance from the center of the film. [Al] and [O] are the number densities of Al and O, respectively. The values for layers of opposite z coordinates have been averaged. A layer of height $\Delta z = 1$ Å is used for sampling.

B. Density and coordination number profiles

The partial density profiles for Al and O are plotted in the top panel of Fig. 4 as a function of distance from the center of the slab ($z=0$). The mass density is calculated using layers of height $\Delta z = 1$ Å parallel to the surfaces and the results are averaged over the two half slabs located at positive and negative z values. Note that the term "layers" is used in a purely geometrical sense without implying any crystallographic order or composition. There are two deviations from stoichiometry in the density profiles shown in Fig. 4. First, the density profile for O extends to a slightly larger distance than that for Al at the surface. Second, the Al density profile has a pronounced peak just underneath the surface. This peak is followed by oscillations in the density profile that die out as one moves into the center of the film. This is easy to understand if one considers the surface formation. The formation of the surface results in attractive force on all atoms from the remaining half space of the bulk. When the surface is formed, it is nearly stoichiometric. The total number of broken bonds for all Al atoms is approximately equal to the total number of broken bonds for all O atoms. Therefore, for each surface Al atom, there are one and a half larger number of broken bonds than for each surface O atom. This results in a larger force on Al atoms from the remaining subsurface atoms that pulls them inwards and, on average, in a larger vertical displacement of Al atoms towards the bulk. This explains why the surface has a preference for oxygen atoms over aluminum atoms. The local electrical neutrality in the system is maintained since charges of excess oxygens at the surface are compensated by aluminum enrichment just below the surface. An alternative explanation for oxygen termination can be put forward based on Pauling's classic rules on ionic crystals.[23] According to the first rule the coordination number of the cation is determined by the cation-anion radius ratio, which is 0.41 for Al-O. According to these empirical rules, Al can occur in both octahedral and tetrahedral coordinations in Al_2O_3. Thus, the Al ion being smaller in size and having a higher net charge than the O ion, it has a higher coordination number. As discussed before, the majority of the Al atoms in our system have tetrahedral coordination, with Al sitting in the center of the tetrahedron. In a tetrahedron occurring at the surface, Al has to be subsurface since at least one of the corner oxygen atoms will be above the center. The predominance of oxygen at the outermost surface has previously been reported in amorphous silica surface simulations.[24,25]

Plotted in the bottom panel of Fig. 4 is the quantity $\Delta n = 3/2[\mathrm{Al}]-[\mathrm{O}]$ that provides a measure of local stoichiometry as a function of z. The quantities [Al] and [O] are the number densities of Al and O, respectively. A value of $\Delta n = 0$ corresponds to perfect stoichiometry whereas $\Delta n > 0$ ($\Delta n < 0$) indicates Al (O) enrichment. The aluminum enrichment below the surface and the oxygen excess at the surface are represented by the positive and the negative values of Δn, respec-

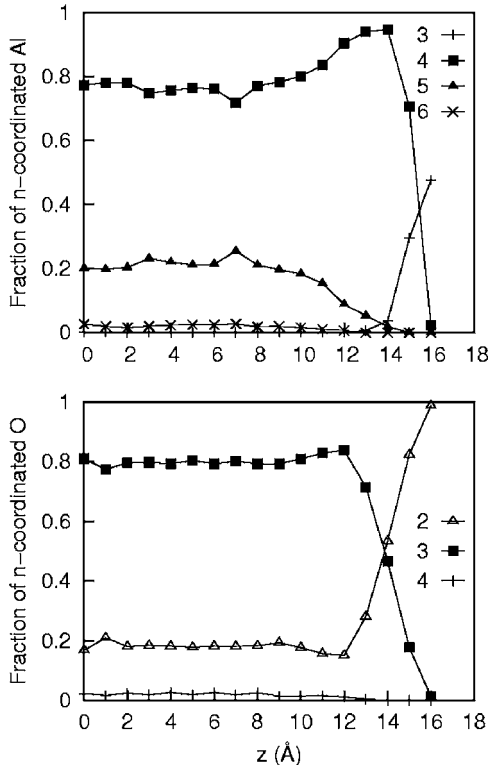

FIG. 5. Profiles of fraction of differently coordinated Al (top) and O (bottom) in the z direction as a function of distance from the center of the film. The values for layers of opposite z coordinates have been averaged. A layer of height $\Delta z=1$ Å is used for sampling.

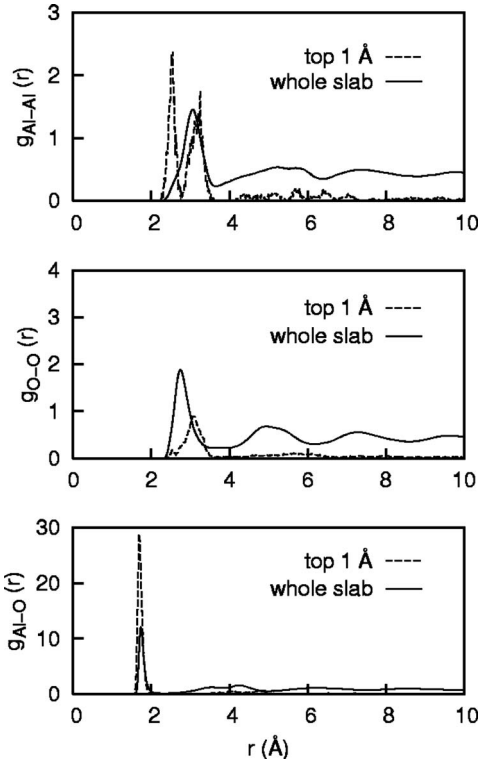

FIG. 6. Partial radial distribution function for Al-Al (top), O-O (center), and Al-O (bottom) pairs. The dashed line represents PRDF for atoms in the top 1 Å thick layer at the surface and the solid line represents PRDF for the whole slab.

tively. As expected, the oscillations in Δn vanish towards the center of the layer. This type of surface segregation has been reported in previous MD simulations of amorphous silica surfaces.[26] In addition, strong inward displacements of surface Al atoms have been predicted also on crystalline alumina surfaces. For example, first principle calculations on both (0001) surface of α- and (001) surface of κ alumina have indicated strong inward relaxations.[11,27] These relaxations are stronger in the case of (001) κ-alumina and result in O-terminated surfaces. This effect was explained on the basis that cation vacancies caused by tetrahedrally coordinated Al make the κ-alumina (001) surfaces more open as compared to α-alumina (0001) surfaces allowing a huge inward relaxation of Al atoms and thus making the surface O terminated. Therefore, the surface oxygen excess appears to be a general property of both amorphous and crystalline alumina surfaces, when the structure of the subsurface layer allows a very strong inward Al relaxation resulting in an O termination.

Further insight into the effect of surface on short range order can be obtained by analyzing the coordination numbers of Al and O atoms. The coordination number is computed using a cutoff of 2.1 Å for the Al-O bond distance, which corresponds to the first minimum in the $g_{\text{Al-O}}$ for the bulk case. The fractions of $n=3,4,5$, and 6 coordinated aluminum atoms (top panel, Fig. 5) and $n=2$, 3, and 4 coordinated oxygen atoms (bottom panel, Fig. 5) are plotted as functions of distance from the center of the slab. The surface has a substantial fraction of three-coordinated Al that disappears for distances below 14 Å from the slab center. The profile of four-coordinated Al increases from zero at the surface to a maximum of 0.94 at 14 Å from the slab center and eventually assumes the bulk value (0.77) below 10 Å from the center. The profiles for five- and six-coordinated Al gradually increase as well, from zero at the surface to the respective bulk values at distances from the center below 10 Å. The presence of excessive four-coordinated Al just below the surface is explained by aluminum enrichment near the surface due to lower number of available O neighbors as compared to the bulk that favors lower coordinated Al at the expense of five- and six-coordinated ones. Oxygen atoms at the surface are predominantly two-coordinated and hence form bridging configurations. The fraction of two-coordinated oxygen atoms decreases parallel with an increase in three-coordinated O and these assume bulk values below 10 Å from the center. Thus, in terms of coordination numbers, surface effects are present as deep as 5 Å below the outermost layer.

C. Radial distribution function

In Fig. 6, distributions $g_{\text{Al-Al}}$ (top panel), $g_{\text{O-O}}$ (center panel), and $g_{\text{Al-O}}$ (bottom panel) for the top surface layer of 1 Å thickness and for the whole slab are compared. The PRDF for the top 1 Å layer included atom pairs only if both atoms belong to the layer. The distribution $g_{\text{Al-Al}}$ for the surface layer has an additional peak at 2.53 Å appearing much before the first peak for $g_{\text{Al-Al}}$ for the whole system at 3.13 Å. For comparison, the first $g_{\text{Al-Al}}$ peak in α alumina is

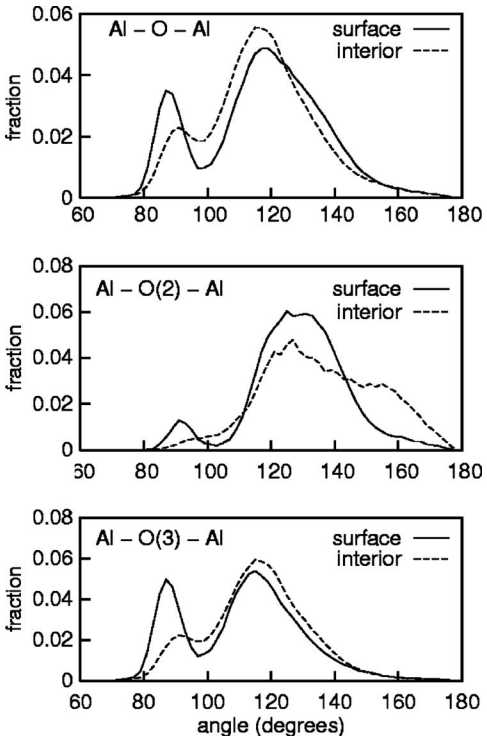

FIG. 7. Al-O-Al bond angle distribution functions for 3 Å thick surface (solid line) and interior (dashed line) layers.

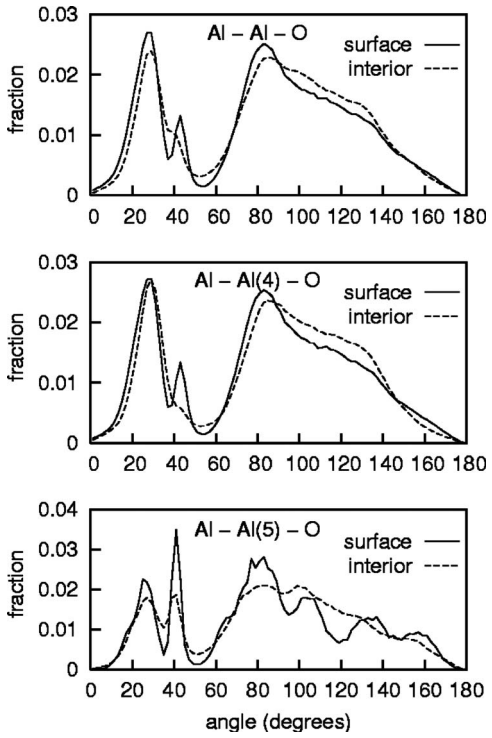

FIG. 8. Al-Al-O bond angle distribution functions for 3 Å thick surface (solid line) and interior (dashed line) layers.

at 2.61 Å and the second peak is located at 3.25 Å. This additional peak at 2.53 Å is due to the preference for edge sharing configurations at the surface. An edge sharing conformation is a two-membered ring where two Al tetrahedra share two oxygen atoms. A two-membered ring is characterized by Al-O-Al and O-Al-O angles of 90° and both O-O and Al-Al first neighbor distances that are shorter than the respective average distances. The distribution $g_{\text{O-O}}$ for the surface layer has the first peak shifted to 3.01 Å as compared to 2.77 Å for the whole system. Also, the first peak of $g_{\text{O-O}}$ for the surface layer has a small shoulder at 2.55 Å. The appearance of this shoulder corresponds to edge sharing configurations. Finally, the first peak of the distribution $g_{\text{Al-O}}$ corresponding to nearest neighbor Al-O distance is at 1.71 Å for the surface layer and the corresponding peak for the whole system is at 1.75 Å. The shorter bond length in the surface layer is a result of higher fractions of three- and four-coordinated Al at the surface. In summary, the PRDF analysis for the surface layer provides evidence for enhanced local ordering characterized by edge-sharing Al tetrahedra.

D. Angle distribution functions

Further information on the short range order near the surface is obtained from the distributions of angles between three neighboring atoms. Two atoms, α and β, are considered neighbors if the distance between them is smaller than a certain cutoff distance. The cutoff distances are chosen to be 3.7, 2.1, and 3.2 Å for Al-Al, Al-O, and O-O pairs, respectively, which correspond to the respective minima in the bulk PRDFs. In Figs. 7 and 8, angle distribution functions for 3-Å thick layers from the surface and from the center of the film are compared. A particular sequence of three atoms is included in the sampling for a layer if the center atom in the sequence belongs to that particular layer. The Al-O-Al bond angle distribution function (Fig. 7 top panel) for the interior has a main peak at 120° and a small peak at around 90°. As was pointed out by Gutierrez *et al.*[12] based on the bulk simulations, the 120° peak corresponds to the corner-sharing Al tetrahedra configuration. The smaller peak at 90° corresponds to edge-sharing configurations. The distribution for the surface layer has a more prominent peak at 90° indicating that edge-sharing configurations are more preferred at the surface than in bulk. In the center and bottom panels of Fig. 7 these distributions are drawn separately for two-coordinated [Al-O(2)-Al] and three-coordinated [Al-O(3)-Al] oxygen atoms in the Al-O-Al sequence, respectively. The Al-O(2)-Al angle distribution for the interior has a peak at 127°. The distribution for the surface layer has a main peak at 131° and a small shoulder at 90°. Also, the distribution profile is more compact around the 131° peak for the surface layer as compared to the interior for which the profile is more spread and extends towards 180°. The Al -O(3)-Al angle distribution for the interior has a main peak at 117° and a smaller peak at 93°. The corresponding distribution for the surface layer has a main peak at 113° and a smaller peak at 87°. However, the peak around 90° is more prominent for the surface layer as compared to the interior. The following can be inferred from these component angle distribution functions. First, although corner sharing configurations are preferred over edge sharing configurations both in the bulk and at the surface, the edge-sharing configurations occur with a higher probability at the surface than

in the bulk. Second, in the bulk as well as on the surface, three-coordinated O is preferred over two-coordinated O in edge-sharing Al-O-Al sequences. Third, there is a small probability that two-coordinated O takes part in edge-sharing Al-O-Al sequences at the surface. This probability is higher for the surface than for the interior.

A similar analysis for the Al-Al-O angle distribution function is presented in Fig. 8. As illustrated by the Al-Al-O angle distribution in the top panel of Fig. 8, the profile for the surface has a very prominent peak at 45° which is present only as a shoulder to the 30° peak in the case of the interior. As pointed out in Ref. 12, the 45° and 30° Al-Al-O peaks are attributed to edge and corner sharing Al tetrahedra, respectively. This indicates that the edge sharing Al tetrahedral configurations are more preferable at the surface than at the interior. The component distribution functions Al-Al(4)-O (center panel) and Al-Al(5)-O (bottom panel) for four- and five-coordinated Al in the center of the Al-Al-O sequence imply the following. First, in the bulk as well as at the surface five-coordinated Al is preferred over four-coordinated O in edge-sharing Al-Al-O sequences. Second, edge-sharing configurations occur with a higher probability at the surface than in the bulk. Third, an Al-Al-O sequence with a 4-coordinated Al in the center takes part in edge-sharing configurations only at the surface.

IV. DISCUSSION

It is useful to compare our results with previous studies on alumina surfaces. The two investigations that involved amorphous alumina surfaces studied oxidation of aluminum nanoparticles.[28,29] It is important to point out that in the oxidation studies of aluminum the stoichiometry of the sample is not fixed and oxidation proceeds from the surface to the interior of the nanoparticles, which leads to a variation of spatial densities of oxygen and aluminum atoms. In contrast, the oxide surfaces in our simulations are formed from a bulk stoichiometric oxide of uniform spatial density, therefore some differences are to be expected. Campbell *et al.*[28] investigated dynamics of oxide formation on Al nanoparticles using molecular dynamics. They found the average mass density in the oxide to be 75% of the α-alumina density (2.9 g/cm^3) and a mixed tetrahedral/octahedral bonding with a predominance of tetrahedral bonding, in comparison with our observations of predominantly tetrahedral bonding in amorphous alumina of 3.23 g/cm^3 density prepared from melt. Their average aluminum coordination in the interior of a 4 nm oxide scale was found to be 3.9 and slightly higher, 4.3, in the 13.3 Å layer at the alumina-environment interface. The Al coordination number in our simulations was found to be 3.3 for the top 3 Å layer and 4.25 for the interior. A proper comparison of coordination numbers with the previous study[28] is quite difficult due to the different geometry of the system, but the numbers around 4 give additional evidence for predominance of tetrahedral bonding. Alavi *et al.*[29] have studied the structures of aluminum oxide bulk phases and oxidation of Al nanoparticles by MD and found that, in the case of Al_1O_1 or higher oxygen content, an oxygen shell forms on the surface of the nanoparticles, which prevents their fragmentation. Thus, our structure of amorphous surfaces, which also has oxygen termination, bears qualitative similarity to amorphous alumina surfaces resulting from aluminum oxidation.

Comparison of our results to previously studied surfaces of crystalline aluminas indicates more similarity with transition aluminas than with α-alumina. DFT calculations of Pinto *et al.*[30] of reconstructions on model γ-alumina crystal surfaces found surface energies of 1.00 ± 0.05 J/m^2 for both (111) and (001) surfaces. This is similar to the surface energies of 0.88 J/m^2 of our amorphous samples. In their study, the (001) surface is highly reconstructed with large aluminum displacements inwards and is dominated by five-coordinated Al, with some tetrahedral Al. The (111) surface exhibits two reconstructions, both with three-coordinated Al surface atoms. The subsurface Al is found to be five coordinated, while top oxygen layers are twofold coordinated. Thus, the coordination of the surface Al atoms on γ-alumina varies between 3 and 5, whereas it is mostly 3 and 4 in our study of amorphous surfaces. Calculations of the relaxed (001) surface[27] of κ-alumina also show oxygen termination and nearly trigonal arrangement of the topmost aluminum atoms.

The (0001) surface of α-alumina is well studied theoretically and has been shown to have aluminum termination with a strong inward relaxation. While significant inward relaxation of Al atoms is a general trend in crystalline alumina surfaces, the oxygen termination of the surface is an effect observed on transition alumina surfaces where the cation vacancy structure allows such a reconstruction. In this respect, the (0001) α-alumina surface has much less in common with amorphous alumina surface, and it also has a higher energy. The present work has focused on dry amorphous alumina surfaces. It is well known that both anodized and ALD alumina contain hydroxyl groups. It would be of great interest to investigate the effect of hydroxyl groups on the surface structure. For example, Hass *et al.*[31] found stable surface reconstructions on OH-covered α-alumina that expose OH groups rather than aluminum atoms. Since we have not included hydrogen or OH groups in the present studies, there is no direct way to compare the results. In the future, we will focus on including hydroxyl groups into the model since they are expected to play an important role in determining the structure and reactivity of amorphous aluminas obtained by ALD and anodization processes.

V. CONCLUSIONS

In this paper, we have investigated the structural properties of amorphous alumina surfaces using MD simulations. The key effect of surface formation is reflected in the density profiles across the film. Oxygen is preferred at the surface and this excess oxygen causes Al enrichment just below (<2 Å) the surface. The excess oxygen and subsequent Al enrichment result in interesting features near the surface in terms of coordination number and short range order. There is a presence of three-coordinated Al atoms at the surface and a higher concentration of two-coordinated O atoms as compared to the bulk. Various angle and partial radial

distribution functions indicate that edge sharing Al tetrahedra configurations are preferred at the surface compared to the bulk. The strong inward relaxation of Al atoms and decreased average coordination are general features of both crystalline and amorphous alumina surfaces. However, the coordination number distribution and structural features, are different for amorphous and crystalline alumina surfaces, and will probably affect the functionality of the amorphous alumina surfaces in technological applications.

ACKNOWLEDGMENTS

This work was supported by the U.S. Department of Energy's Office of Basic Energy Sciences under Contract No. W-31-109-ENG-38. Use of computer resources from Argonne National Laboratory Computer Resource Center and U.S. DOE National Energy Research Supercomputer Center is gratefully acknowledged.

*Corresponding author. Electronic address: zapol@anl.gov

[1] J. P. O'Sullivan and G. C. Wood, Proc. R. Soc. London, Ser. A **317**, 511 (1970).
[2] G. Xiong, J. W. Elam, H. Feng, C. Y. Han, H.-H. Wang, L. E. Iton, L. A. Curtiss, M. J. Pellin, M. Kung, H. Kung, and P. C. Stair, J. Phys. Chem. B **109**, 14059 (2005).
[3] M. J. Pellin, P. C. Stair, G. Xiong, J. W. Elam, J. Birrell, L. Curtiss, S. M. George, C. Y. Han, L. Iton, H. Kung, M. Kung, and H.-H. Wang, Catal. Lett. **102**, 127 (2005).
[4] A. W. Ott, K. C. McCarley, J. W. Klaus, J. D. Way, and S. M. George, Appl. Surf. Sci. **107**, 128 (1996).
[5] V. A. Nasluzov, V. V. Rivanenkov, A. M. Shor, K. M. Neyman, U. Birkenheuer, and N. Rosch, Int. J. Quantum Chem. **90**, 386 (2000).
[6] S. D. Elliot, Comput. Mater. Sci. **33**, 20 (2005).
[7] S. M. Levine and A. H. Garofalini, J. Chem. Phys. **86**, 2997 (1987).
[8] G. P. Feuston and S. H. Garofalini, J. Chem. Phys. **91**, 564 (1989).
[9] S. Blonski and S. H. Garofalini, Surf. Sci. **295**, 263 (1993).
[10] A. Marmier and M. W. Finnis, J. Phys.: Condens. Matter **14**, 7797 (2002).
[11] L. J. Alvarez, L. E. Leon, J. F. Sanz, M. J. Capitan, and J. A. Odriozola, Phys. Rev. B **50**, 2561 (1994).
[12] G. Gutierrez and B. Johansson, Phys. Rev. B **65**, 104202 (2002).
[13] G. Gutierrez, Rev. Mex. Fis. **48**, 60 (2002).
[14] V. V. Hoang, Phys. Rev. B **70**, 134204 (2004).
[15] V. V. Hoang and S. K. Oh, Physica B **364**, 225 (2005).
[16] M. Matsui, Miner. Mag. **58A**, 571 (1994).
[17] G. Gutierrez, A. B. Belonoshko, R. Ahuja, and B. Johansson, Phys. Rev. E **61**, 2723 (2000).
[18] K. Refson, Comput. Phys. Commun. **126**, 309 (2000).
[19] J. R. B. Gomes, I. de P. R. Moreira, P. Reinhardt, A. Wander, B. G. Searle, N. M. Harrison, and F. Illas, Chem. Phys. Lett. **341**, 412 (2001).
[20] M. Baudin and K. Hermansson, Surf. Sci. **474**, 107 (2001).
[21] J. M. McHale, A. Auroux, A. J. Perrota, and A. Navrotsky, Science **277**, 788 (1997).
[22] P. Lamparter and R. Kniep, Physica B **234-236**, 405 (1997).
[23] L. Pauling, J. Am. Chem. Soc. **51**, 1010 (1929).
[24] D. A. Litton and S. H. Garofalini, J. Non-Cryst. Solids **217**, 250 (1997).
[25] A. Roder, W. Kob, and K. Binder, J. Chem. Phys. **114**, 7602 (2001).
[26] M. Rarivomanantsoa, P. Jund, and R. Jullien, J. Phys.: Condens. Matter **13**, 6707 (2001).
[27] C. Ruberto, Y. Yourdshahyan, and B. I. Lundqvist, Phys. Rev. B **67**, 195412 (2003).
[28] T. Campbell, R. K. Kalia, A. Nakano, P. Vashishta, S. Ogata, and S. Rodgers, Phys. Rev. Lett. **82**, 4866 (1999).
[29] S. Alavi, J. W. Mintmire, and D. L. Thompson, J. Phys. Chem. B **109**, 209 (2005).
[30] H. P. Pinto, R. M. Nieminen, and S. D. Elliott, Phys. Rev. B **70**, 125402 (2004).
[31] K. C. Hass, W. F. Schneider, A. Curioni, and W. Andreoni, J. Phys. Chem. B **104**, 5527 (2000).